STAR FORMATION HISTORY SINCE $Z = 1.5$ AS INFERRED FROM REST-FRAME ULTRAVIOLET LUMINOSITY DENSITY EVOLUTION

Gillian Wilson[1], Lennox L. Cowie[2], Amy J. Barger[2,3,4], and D. J. Burke[2,5]

ABSTRACT

We investigate the evolution of the universal rest-frame ultraviolet luminosity density from $z = 1.5$ to the present. We analyze an extensive sample of multicolor data (U'_{AB}, B_{AB}, $V_{AB} = 24.5$) plus spectroscopic redshifts from the Hawaii Survey Fields and the Hubble Deep Field. Our multicolor data allow us to select our sample in the rest-frame ultraviolet (2500 Å) over the entire redshift range to $z = 1.5$. We conclude that the evolution in the luminosity density is a function of the form $(1 + z)^{1.7 \pm 1.0}$ for a flat lambda ($\Omega_{m0} = 0.3, \Omega_{\lambda 0} = 0.7$) cosmology and $(1 + z)^{2.4 \pm 1.0}$ for an Einstein-de Sitter cosmology.

Subject headings: cosmology: observations — galaxies: distances and redshifts — galaxies: evolution — galaxies: formation — galaxies: luminosity function, mass function

1. INTRODUCTION

A major goal of observational cosmology is to understand the star formation history of the Universe from the earliest epoch of structure formation to the present. Much recent attention has focused on determining the contribution to the global history from the most distant sources; however, the star formation history even at modest redshifts ($z < 1$) is not well determined and has recently undergone a revision.

Early work by Madau et al. (1996) (later updated by Madau, Pozzetti, & Dickinson 1998) suggested that the global star formation as seen in the optical and ultraviolet (UV) had a strong peak around $z = 1$ and then fell very steeply at lower redshifts. The $z < 1$ data used in the analysis were taken from a paper by Lilly et al. (1996),

who used rest-frame near-UV luminosities derived from the I-selected Canada-France Redshift Survey (CFRS, Lilly et al. 1995) to determine the comoving UV luminosity density from $z = 1$ to the present. These authors found the evolution to be a steep function of the form $(1 + z)^4$. However, when Treyer et al. (1998) presented the first UV-selected constraints on the local integrated luminosity density, they found that their result was well above the optically-derived estimates. Sullivan et al. (2000) subsequently tripled the Treyer et al. UV-selected sample and confirmed the higher local volume-averaged star formation rate.

Cowie, Songaila, & Barger (1999, hereafter CSB) decided to reinvestigate the rest-frame UV luminosity density evolution to $z = 1$ using a large, extremely deep, and highly complete spectroscopic galaxy redshift survey. Their data enabled them to select objects based on the rest-frame UV magnitudes at all redshifts. The evolution found by these authors was a much shallower function of the form $(1 + z)^{1.5}$. CSB suggested that the differences between their results and those of Lilly et al. could be accounted for by the I-band selection of the Lilly et al. sample, which required large extrapolations to obtain UV colors, and by

[1] Physics Department, Brown University, 182 Hope Street, Providence, RI 02912

[2] Institute for Astronomy, University of Hawaii, 2680 Woodlawn Drive, Honolulu, HI 96822

[3] Department of Astronomy, University of Wisconsin-Madison, 475 North Charter Street, Madison, WI 53706

[4] Hubble Fellow and Chandra Fellow at Large

[5] Harvard-Smithsonian Center for Astrophysics, 60 Garden Street, Cambridge, MA 02138

the CFRS data not being deep enough to probe the flat segments of the luminosity function (LF), which meant that at redshifts near $z = 1$, reliable extrapolations to total luminosity density could not be made.

In this paper, we expand on the work of CSB to more thoroughly investigate the rest-frame UV luminosity density evolution from $z = 1.5$ to the present. Our new galaxy sample is nearly twice as large as that used by CSB, and we explore various methods for constructing the UV LFs. The outline of the paper is as follows. In § 2 we present our data sample and strategy and we investigate the U' number counts and redshift distribution. We also explore the redshift-magnitude relationship for the U', B, and V passbands. In § 3 we describe how we construct rest-frame UV LFs as a function of redshift from the U', B, and V data. In § 4 we utilize these LFs to infer the evolution of the global UV luminosity density with redshift. In § 5 we summarize our conclusions. Initially, we assume a flat lambda ($\Omega_{m0} = 0.3, \Omega_{\lambda0} = 0.7$) cosmology with $H_0 = 100$ h km s^{-1} Mpc^{-1}. Subsequently, we investigate the effect of an Einstein-de Sitter ($\Omega_{m0} = 1.0, \Omega_{\lambda0} = 0.0$) cosmology on our results.

2. OBSERVATIONS

We analyzed a three passband subset (U' (3400 ± 150Å), B, V) of an ongoing eight passband (U', B, V, R, I, Z, J, HK') Hawaii imaging survey of four $6' \times 2.5'$ areas crossing the Hawaii Survey Fields SSA13, SSA17, and SSA22 (Lilly, Cowie, & Gardner 1991) and the Hubble Deep Field (HDF) (Williams et al. 1996). The B and V images were obtained using the Low-Resolution Imaging Spectrograph (LRIS; Oke et al. 1995) on the Keck 10 m telescopes and the UH8K CCD Mosaic Camera (Luppino 1997) on the Canada-France-Hawaii 3.6 m telescope. The U' data were taken with the ORBIT CCD on the University of Hawaii 2.2 m telescope. All magnitudes were measured in $3''$ diameter apertures and corrected to total magnitudes following the procedures described in Cowie et al. (1994).

The sources analyzed in this paper contain and extend the CSB catalogs. The total number of galaxies with spectroscopic redshifts in the present U', B, and V samples are 403, 414, and 518, all to a survey limit magnitude (AB) of 24.5. These numbers can be compared to those in CSB (218, 350, and 259 respectively) . Thus, our current dataset contains approximately double the number of objects in the CSB U' and V samples.

The great advantage of multiband data is that one can, for all redshifts, select galaxies based on their rest-frame UV magnitudes, thereby avoiding the uncertainties associated with selecting galaxies at longer (redder) wavelengths and then extrapolating to obtain their UV magnitudes. In addition, the depth of the current dataset allows us to construct LFs to sufficiently faint absolute magnitudes to constrain the faint-end slope. Moreover, by selecting galaxies based on their rest-frame UV magnitudes, we expect the relative shape of the inferred UV LFs to be minimally sensitive to the effect of interstellar dust; i.e., we expect the relative forms of our derived LFs (and hence the relative values of our luminosity densities) to be subject only to evolution in the amount or properties of galactic dust with redshift and not to its effect in absolute terms. (Note that any extinction due to dust in the source galaxy should not be confused with the tiny extinction corrections due to interstellar dust)

As discussed in CSB, one is free to choose the rest-frame wavelength at which to compute LFs and the UV light density. For our dataset, 2500 Å provides a sensible compromise between our wide range of redshifts and large number of galaxies in each passband.

Because there are missing or unidentified galaxies in each sample, we construct LFs by either omitting them (i.e., we assume they are unidentified because they are unusual in some way, e.g., at very high redshift), or by assuming they are distributed in redshift in exactly the same manner as the identified galaxies (i.e., we assume they are identical to the measured galaxies but have been missed for some trivial reason). It is likely that the true LF lies between these two possibilities. In subsequent sections we refer to the former case as minimal and the latter case as incompleteness-corrected. The U', B, and V samples are 88%, 90%, and 83% complete, respectively, so the correction is not a huge factor in any case.

2.1. The U' Sample

Figure 1 shows number counts versus apparent magnitude for our U' sample. The symbols indicate the number counts in each of the four fields. We assume a 1 σ Poisson uncertainty for each field. The solid line shows the best-fit to the counts for galaxies with magnitudes between U' of 22.0 and 24.0 (slope of 0.61 ± 0.06 and intercept at -10.34 ± 1.49). The uncertainties were calculated from the field-to-field variations.

A number of groups (e.g., Williams et al. 1996; Pozzetti et al. 1998; Gardner, Brown, & Ferguson 2000) have measured deep galaxy counts at 3000 Å from the *HST* Hubble Deep Field imaging survey, but their counts are somewhat deeper than those presented here, so it is difficult to make a direct comparison. The sample most similar to ours was that obtained at the Palomar 5 m by Hogg et al. (1997). We overplot their data (filled diamonds) on Fig. 1 for comparison, after converting their magnitudes to U'_{AB} by adding 0.79 mag. The agreement is generally good.

In Fig. 2 we show the total number of objects in our U' sample versus redshift for two apparent magnitude bins. The upper panel shows the number of galaxies versus redshift for all galaxies with U' between 22.5 and 23.5, and the lower panel is for galaxies with U' between 23.5 and 24.5.

Wilson et al. (2001) found that a good model for the redshift distribution (at least at I and V) is provided by

$$p(z) = 0.5z^2 \exp(-z/z_0)/z_0{}^3 \qquad (1)$$

where $p(z) \times dz$ is the probability of finding a galaxy in the redshift interval $z + dz$ (the mean redshift is $\overline{z} = 3z_0$ and the median redshift is $z_{median} = 2.67z_0$). A nice property of (1) is that there is only one free parameter, the redshift scale parameter, z_0. The solid lines overlaid on Fig. 2 show the best-fits to the model ($z_0 = 0.19$ and $z_0 = 0.28$), normalized to the total number of galaxies in each sample.

2.2. Magnitude-Redshift Dependence

In this section we investigate the dependence of median redshift on apparent magnitude and wavelength. In Fig. 3 we show redshift versus magnitude for the U' sample. The symbols denote the field in which the galaxy was observed. Note that
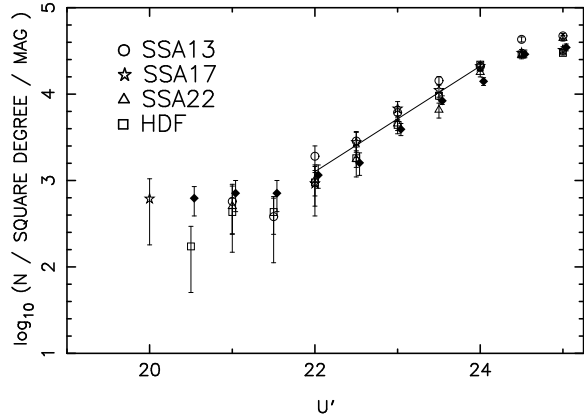

Fig. 1.— Number counts versus apparent magnitude for the U' sample. The four fields are as indicated by the key. The solid line shows the best-fit to the counts between U' of 22.0 and 24.0 (slope of 0.61 and intercept at -10.34). The filled diamonds are the counts from Hogg et al. (1997).
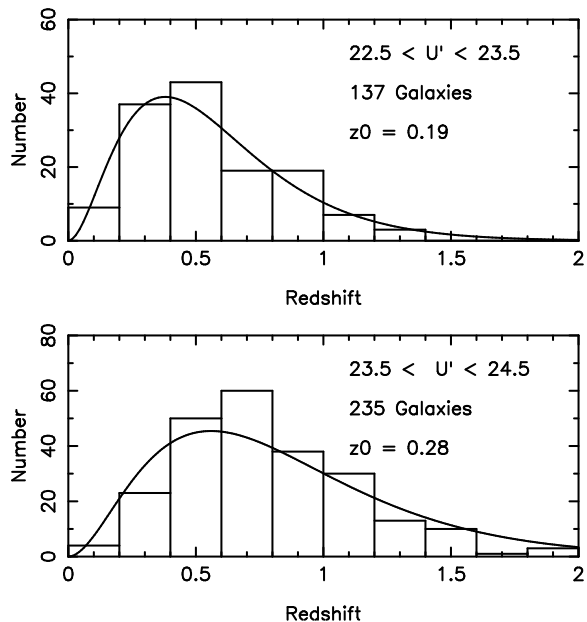

Fig. 2.— Redshift distributions for the U' sample. The upper panel shows $N(z)$ for a one magnitude wide band ($22.5 < U' \leq 23.5$) in apparent magnitude. At this depth the data are 97% complete. The solid line shows the best-fit to the model (Eq. 1) with redshift scale parameter 0.19. The lower panel shows $N(z)$ for $23.5 < U' \leq 24.5$. At this depth the data are 87% complete and best-fit with redshift scale parameter 0.28.

TABLE 1

MEDIAN REDSHIFTS AND GALAXY NUMBERS AS A FUNCTION OF APPARENT MAGNITUDE AND
WAVELENGTH (THE UNCERTAINTIES ARE 1 σ POISSONIAN LIMITS).

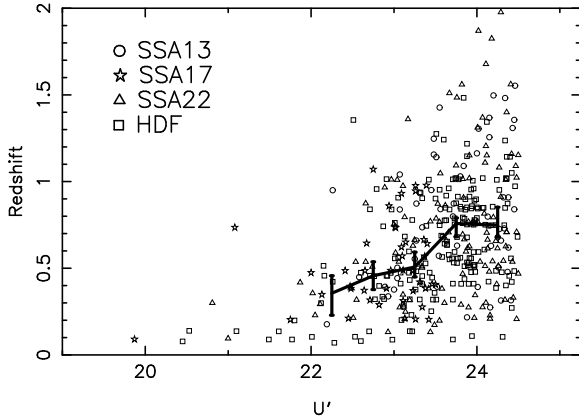| Mag.	$z_{\mathrm{med}}(U')$	$N(U')$	$z_{\mathrm{med}}(B)$	$N(B)$	$z_{\mathrm{med}}(V)$	$N(V)$
22.25	$0.356\,^{0.457}_{0.229}$	17	$0.380\,^{0.452}_{0.317}$	44	$0.411\,^{0.471}_{0.348}$	45
22.75	$0.457\,^{0.537}_{0.377}$	43	$0.475\,^{0.560}_{0.432}$	55	$0.475\,^{0.524}_{0.455}$	65
23.25	$0.507\,^{0.593}_{0.450}$	94	$0.663\,^{0.777}_{0.564}$	86	$0.626\,^{0.742}_{0.531}$	113
23.75	$0.758\,^{0.790}_{0.682}$	127	$0.715\,^{0.788}_{0.617}$	112	$0.680\,^{0.753}_{0.615}$	141
24.25	$0.748\,^{0.852}_{0.680}$	108	$0.753\,^{1.010}_{0.562}$	77	$0.850\,^{0.980}_{0.709}$	104

Fig. 3.— Galaxy redshift versus apparent magnitude for the U' sample. The key is as in Fig. 1. The solid line shows the median redshift and the 1 σ Poisson uncertainties (Table 1).

the SSA13, SSA22, and HDF fields are $\sim 90\%$ complete to an AB limiting magnitude of 24.5, and the SSA17 field is similarly complete to 23.5.

Table 1 quantifies Fig. 3, giving the median redshift with $\pm$ 1 σ Poisson uncertainties (Gehrels 1986) and the number of objects in each half-magnitude interval as a function of apparent magnitude. We note that the median redshift obtained from the parameterized fit to the data (Eq. 1) for the $22.5 < U' \leq 23.5$ interval is 0.51, and for the $23.5 < U' \leq 24.5$ interval, 0.75. The values are in good agreement with those calculated directly in Table 1.

In Table 1 we also calculate the median redshift for the B and V samples. Median redshift as a function of apparent magnitude can potentially be used to constrain galaxy evolution models, e.g. if we compare with the B-band predictions from the merger model proposed by Carlberg (1992, his Table 2), we find that his median redshift values of 0.44 for $B = 23$ and 0.55 for $B = 24$ are lower than our values, suggesting that more pure luminosity evolution might have occurred than was proposed in his model.

3.   THE REST-FRAME ULTRAVIOLET LUMINOSITY FUNCTION

For any given galaxy, i, at redshift, z, the equation relating the absolute and apparent magnitudes is given by

$$M_i^{2500} = m_i - 5\log d_L(z_i) - 25 + 2.5\log(1+z) + dK(z_i) \tag{2}$$

4

where m is the observed magnitude at the red-shifted wavelength and $d_L(z)$ is the luminosity distance in h^{-1} Mpc. $dK(z)$ is given by

$$dK(z) = 2.5 \log_{10} \frac{f_\nu[2500\text{Å} \times (1+z)]}{f_\nu[2500\text{Å} \times (1+z_c)]} \quad (3)$$

where f_ν is the spectral energy distribution of the galaxy and z_c is the redshift corresponding to the center of the band. $dK(z)$ is a differential K-correction to account for each sample containing a range of redshifts and hence a range of rest-frame wavelengths around 2500 Å. It is generally small and is obtained by interpolation from the neighboring passbands.

3.1. Luminosity Functions from the $V_{\max}$ Method

We used two methods to construct LFs: the traditional $V_{\max}$ method described by Schmidt (1968), Felten (1976), and Ellis et al. (1996) and a new method recently suggested by Page & Carrera (2000). In the $V_{\max}$ method, the number density of galaxies in the redshift range $[z_1, z_2]$ with absolute magnitude M is given by

$$\phi(M)\,dM = \sum \frac{1}{V_{\max}(M)} \quad (4)$$

where the sum is over the galaxies in the magnitude interval $M \pm dM/2$. $V_{\max}(M)$ is the maximum total comoving volume within which each galaxy (as defined by its apparent magnitude and redshift) would remain detectable within survey limits. The uncertainty for each magnitude interval is conventionally calculated from

$$\sigma = \left[\sum \frac{1}{(V_{\max}(M))^2} \right]^{\frac{1}{2}} \quad (5)$$

(Marshall 1985; Boyle, Shanks, & Peterson 1988). This expression weights each observation by its contribution to the sum. However, it assumes Gaussian statistics, which is not ideal for bins at the bright or faint end of the LF where only a small number of objects contribute to the sum.

Figure 4 shows the 2500 Å rest-frame LF for our three redshift bins: $z = 0.2 - 0.5$, constructed from the U' sample (upper panel), $z =$

0.6 − 1.0, constructed from the B sample (center panel), and $z = 1.0 − 1.5$, constructed from the V sample (lower panel). At redshifts $z = 0.35 \pm 0.15$, 0.80 ± 0.20 and 1.25 ± 0.25, the U' (3400Å), B (4500Å) and V (5500Å) samples correspond to rest-wavelengths of 2519^{+314}_{-253}, 2500^{+312}_{-250} and 2444^{+306}_{-244} Å. The open circles denote the minimal function, and the solid circles denote the incompleteness-corrected function. The number of galaxies used in the construction of each LF was 121 (U'), 119 (B), and 59 (V).

3.2. Luminosity Functions from the PC Method

The Page & Carrera (2000) method is very similar to the $V_{\max}(M)$ method in that it results in a binned differential LF, but the advantage is that it more accurately determines the LF at the faint end. The maximum redshift at which any galaxy may be found is a constantly varying function determined by the flux limit of the survey. The $V_{\max}(M)$ method assumes that the redshift is a constant for any given absolute magnitude bin. However, by dividing each magnitude bin into a series of steps, calculating $V_{\max}(M)$ for each interval, and then integrating over the magnitude bin, one can obtain a more precise estimate of the maximum volume to which each object could be observed in the survey. Estimates of $\phi(M)$ obtained by either of the two methods should agree at the bright end of the LF where objects are much brighter than the flux limit. The two estimates should also agree in the case of very fine magnitude intervals, such that the widths of the magnitude bins tend to zero.

We denote the LFs obtained using the V_{PC} method by diamonds in Fig. 4. The open triangles show the minimal function and the solid triangles show the incompleteness-corrected function. The diamonds have been offset from the circles of the $V_{\max}$ method by 0.15 mag for clarity. The ± 1 σ Poisson uncertainties (Gehrels 1986) in the LFs are appropriate for small numbers of objects per magnitude interval. The LFs obtained from the two methods are very similar.

Both $V_{\max}(M)$ and $V_{\text{PC}}(M)$ give unbiased estimates of $\phi(M)$ only if galaxy clustering can be neglected. It is easy to imagine how a nearby excess of clustering could bias the estimator: such
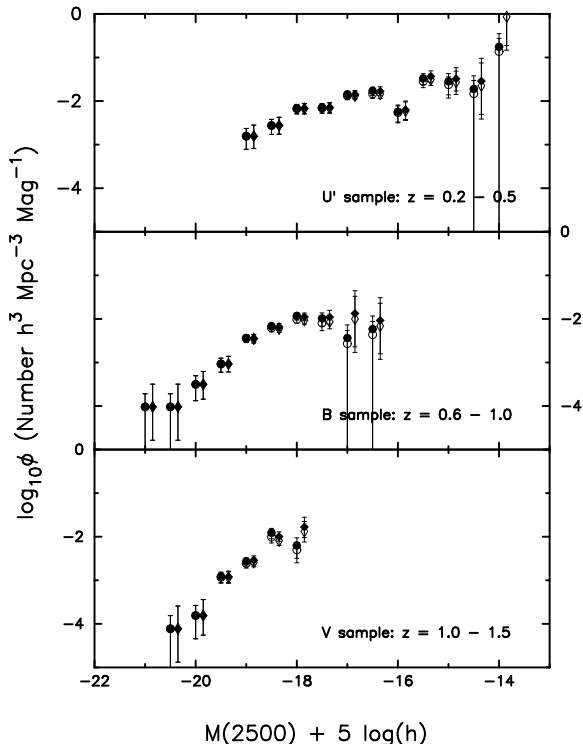
Fig. 4.— The 2500 Å rest-frame luminosity function for three redshift bins: $z = 0.2 - 0.5$, from the U' sample (upper panel), $z = 0.6 - 1.0$, from the B sample (center panel), and $z = 1.0 - 1.5$, from the V sample (lower panel). An $\Omega_{m0} = 0.3, \Omega_{\lambda 0} = 0.7$ cosmology is assumed. The open circles denote the minimal function, and the solid circles denote the incompleteness-corrected function obtained using the V_{max} method. The diamonds (offset by 0.15 mag for clarity) show the minimal (open) and incompleteness-corrected (solid) functions obtained using the V_{PC} method. See text for details and an explanation of the uncertainties. For this dataset the luminosity functions obtained from the two methods are very similar.

an excess of intrinsically faint galaxies would cause the LF to be too steep at the faint end. Although the effects of clustering are mostly of concern in pencil-beam surveys, we tested two maximum likelihood alternatives, which should be less sensitive to clustering, on our U' sample. These were the Schechter fit estimator suggested by Sandage, Tammann, & Yahil (1979) and the stepwise estimator of Efstathiou, Ellis, & Peterson (1988). In all cases, the LFs were very similar to those obtained using V_{max}, giving us confidence in the robustness of our results. We also note that the LFs in this paper were obtained using code written independently from that used in CSB.

3.3. Schechter Parameterization

We then assumed that each LF could be parameterized by a Schechter function

$$\phi(M)\, dM = k\phi^\star e^{k(\alpha+1)(M^\star - M)} e^{-e^{k(M^\star - M)}}\, dM \tag{6}$$

where $k = \frac{2}{5}\ln 10$ (Schechter 1976). We solved for the best-fit Schechter parameters assuming two fixed faint-end slopes that likely bound the range of faint-end slopes : $\alpha = -1.0$ and $\alpha = -1.5$. Table 2 shows the best-fit absolute magnitude at the knee, $M^\star$, and normalization, $\phi^\star$ for these values of fixed faint-end slope. In Fig. 5 the open circles again show the minimal function; the solid circles the incompleteness-corrected function assuming a flat lambda cosmology as in Figure 4. Overlaid on Fig. 5 are the best-fitting Schechter functions assuming $\alpha = -1.0$ or $\alpha = -1.5$. The solid portion of the line shows the magnitude range utilized in the fit.

3.4. Effect of Cosmology

We then investigated how one's choice of cosmology affects the LFs. We reconstructed LFs again using the $V_{max}(M)$ method but this time assuming an Einstein-de Sitter cosmology. For comparison, in Fig. 5, the open triangles show the minimal function; the solid triangles the incompleteness-corrected function assuming this cosmology. As in Figure 4, the triangles have been offset by 0.15 mag for clarity.

Table 3 shows the best-fit Schechter values of absolute magnitude at the knee $(M^\star)$ and normalization $(\phi^\star)$ for the Einstein-de Sitter cosmology

6

TABLE 2

SCHECHTER FUNCTION PARAMETER FITS FOR MINIMAL AND INCOMPLETENESS-CORRECTED POINTS FOR FLAT LAMBDA COSMOLOGY. THE COLUMNS SHOW THE BEST-FIT VALUES OF ABSOLUTE MAGNITUDE AT THE KNEE $(M^\star)$, NORMALIZATION $(\phi^\star)$, AND REDUCED χ^2 FOR FIXED FAINT-END SLOPE (α) OF -1.0 AND -1.5.

Sample	Corrected?	$\alpha = -1.0$			$\alpha = -1.5$			Range
		$M^\star$	$\phi^\star$	χ^2/ν	$M^\star$	$\phi^\star$	χ^2/ν	
U'	No	-18.17	0.0142	1.90	-19.86	0.0024	2.51	$[-19.25 : -14.75]$
U'	Yes	-18.08	0.0161	1.25	-19.64	0.0031	1.58	$[-19.25 : -14.75]$
B	No	-18.46	0.0178	0.55	-18.96	0.0089	0.86	$[-21.25 : -17.25]$
B	Yes	-18.34	0.0232	0.20	-18.81	0.0123	0.36	$[-21.25 : -17.25]$
V	No	-18.30	0.0212	0.87	-18.53	0.0183	0.75	$[-20.75 : -18.25]$
V	Yes	-18.12	0.0348	0.69	-18.35	0.0306	0.58	$[-20.75 : -18.25]$

TABLE 3

SCHECHTER FUNCTION PARAMETER FITS FOR MINIMAL AND INCOMPLETENESS-CORRECTED POINTS FOR EINSTEIN-DE SITTER COSMOLOGY. THE COLUMNS SHOW THE BEST-FIT VALUES OF ABSOLUTE MAGNITUDE AT THE KNEE $(M^\star)$, NORMALIZATION $(\phi^\star)$ AND REDUCED χ^2 FOR FIXED FAINT-END SLOPE (α) OF -1.0 AND -1.5.

Sample	Corrected?	$\alpha = -1.0$			$\alpha = -1.5$			Range
		$M^\star$	$\phi^\star$	χ^2/ν	$M^\star$	$\phi^\star$	χ^2/ν	
U'	No	-17.64	0.0322	0.41	-19.02	0.0070	0.88	$[-18.75 : -14.75]$
U'	Yes	-17.52	0.0378	0.22	-18.75	0.0094	0.41	$[-18.75 : -14.75]$
B	No	-17.86	0.0512	0.26	-18.23	0.0318	0.25	$[-20.75 : -17.25]$
B	Yes	-17.75	0.0643	0.09	-18.13	0.0405	0.05	$[-20.75 : -17.25]$
V	No	-17.63	0.0812	0.19	-17.85	0.0699	0.21	$[-20.25 : -17.75]$
V	Yes	-17.54	0.1100	0.04	-17.78	0.0932	0.04	$[-20.25 : -17.75]$

(again assuming fixed faint-end slopes of -1.0 and -1.5). From Figure 5 and from Tables 2 and 3, it is clear that the larger distance/volumes associated with a cosmological constant cause $M^\star$ and $\phi^\star$ to decrease compared to the best-fit parameters in the Einstein-de Sitter case.

4. REST-FRAME UV LUMINOSITY DENSITY EVOLUTION

The LFs in § 3 can now be used to calculate the rest-frame ultraviolet luminosity densities, $\mathcal{L}$, with redshift. One approach is to choose a magnitude limit and to sum the LF over the magnitude bins directly using

$$\mathcal{L}_{\mathrm{Direct}} = 4.4 \times 10^{20} \sum \frac{10^{-0.4M}}{V_{\mathrm{max}}(M)} h \ \mathrm{erg \ s^{-1} \ Hz^{-1} \ Mpc^{-3}}$$

(7)

An alternative approach, which we adopt, is to choose a faint-end slope (we use either $\alpha = -1.0$ or $\alpha = -1.5$) and to integrate the LF analytically using the best-fit Schechter parameters from Tables 2 and 3

$$\mathcal{L}_{\mathrm{Schechter}} = \int_0^\infty L\phi(L)dL = L_\star \phi_\star \Gamma(\alpha + 2) \quad (8)$$

giving

$$\mathcal{L}_{\mathrm{Schechter}} = 4.4 \times 10^{20} \times 10^{-0.4 \ M_\star} \phi_\star \Gamma(\alpha + 2) \ h$$

(9)

in units of ergs $\mathrm{s^{-1} \ Hz^{-1} \ Mpc^{-3}}$. Although this method involves integrating over all luminosities, fainter galaxies have a rapidly decreasing contribution to the total luminosity density, and thus the two methods give similar results. We calculate the luminosity density for both the minimal and incompleteness-corrected cases assuming firstly a faint-end slope of $\alpha = -1.0$ and then $\alpha = -1.5$. The resulting luminosity densities for the flat lambda and Einstein de-Sitter cosmologies are shown in Table 4.

Luminosity density evolution with redshift is often parameterized as a power-law, $\mathcal{L} \propto (1 + z)^\beta$. In Fig. 6, we show $\log_{10}$(luminosity density) versus $\log_{10}(1 + z)$ using the values from Table 4. As in Fig. 5, we use circles to denote the the flat lambda
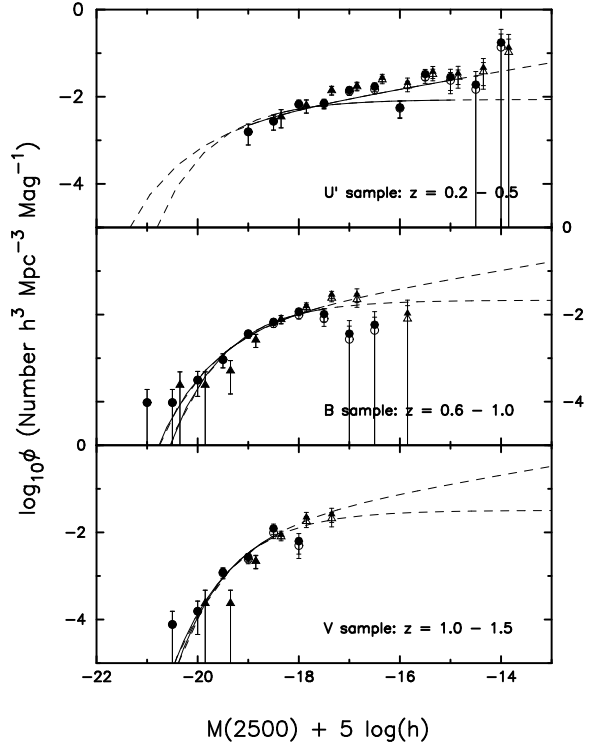

Fig. 5.— Circles as in Fig. 4 for a $\Omega_{m0} = 0.3, \Omega_{\lambda0} = 0.7$ cosmology. Overlaid are the best-fitting Schechter functions assuming either $\alpha = -1.0$ or $\alpha = -1.5$. The solid portion of the line shows the magnitude range utilized in the fit. Also shown and denoted by the triangles (offset by 0.15 mag for clarity) are the minimal (open) and incompleteness-corrected (solid) functions obtained for an Einstein-de Sitter cosmology. See text for details. See Tables 2 and 3 for best Schechter function fit parameters.

8

TABLE 4
COMOVING 2500Å UV LUMINOSITY DENSITY.[a]

| Sample | Redshift | Corrected? | $\log_{10}$(Luminosity Density) | | | |
| | | | Flat Lambda | | Einstein-de Sitter | |
			$\alpha = -1.0$	$\alpha = -1.5$	$\alpha = -1.0$	$\alpha = -1.5$
U'	0.35 ± 0.15	No	26.058	26.211	26.202	26.340
U'	0.35 ± 0.15	Yes	26.077	26.234	26.223	26.360
B	0.80 ± 0.20	No	26.272	26.420	26.491	26.681
B	0.80 ± 0.20	Yes	26.339	26.500	26.546	26.746
V	1.35 ± 0.25	No	26.284	26.561	26.600	26.871
V	1.35 ± 0.25	No	26.428	26.712	26.695	26.968

[a]Units are h ergs s^{-1} Hz^{-1} Mpc^{-3}

cosmology and triangles to denote the Einstein-de Sitter cosmology. The open symbols denote the minimal case , and the solid symbols denote the incompleteness-corrected case.

We solved for the best-fit power-law exponent, β, in each case. We used the mean of the luminosity densities obtained assuming faint end slopes of $\alpha = -1.0$ and $\alpha = -1.5$ as our best estimate, with the extreme values as estimates of the uncertainty. Table 5 gives the best-fit exponent and uncertainty as a function of completeness-correction and cosmology. For the flat lambda cosmology we found a best-fit exponent of 1.44 ± 0.63 in the minimal case and a best-fit exponent of 1.95 ± 0.65 in the incompleteness-corrected case. For the Einstein de-Sitter cosmology we found a best-fit exponent of 2.22 ± 0.62 in the minimal case and a best-fit exponent of 2.54 ± 0.62 in the incompleteness-corrected case. Thus, depending on the choice of completeness correction, we conclude that luminosity density evolves as $(1+z)^{1.7\pm1.0}$ in the $\Omega_{m0} = 0.3, \Omega_{\lambda0} = 0.7$ cosmology and as $(1 + z)^{2.4\pm1.0}$ in the Einstein de-Sitter cosmology. The two solid lines overlaid on Fig. 6 show the best-fit solutions for each cosmology in the incompleteness-corrected case. The Einstein de-Sitter value is slightly steeper than that obtained by CSB (1.3 for $\alpha = -1.0$ and 1.7 for $\alpha = -1.5$) but consistent within the uncertainties.
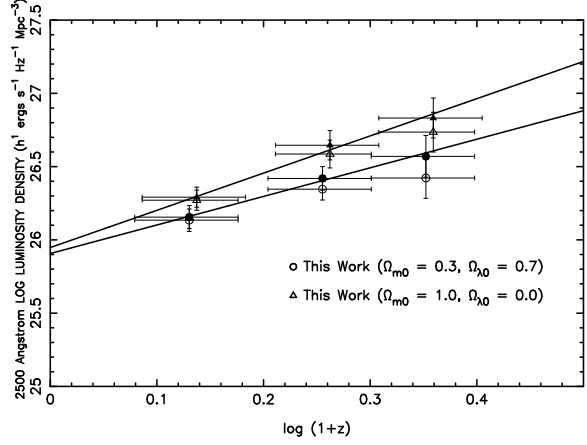
Finally, in Fig. 7 we compare our values of lu-

Fig. 6.— $\log_{10}$(Luminosity density) versus $\log_{10}(1 + z)$. The open circles denote the minimal case and the solid circles denote the incompleteness-corrected case, both for the flat lambda cosmology. The vertical bars show the uncertainties in luminosity density caused by assuming $\alpha = -1.0$ (lower) or $\alpha = -1.5$ (upper). The triangles show same and are for an Einstein de-Sitter cosmology. They have been offset slightly for clarity. Also shown are the best-fit power-law to the incompleteness-corrected values for each cosmology. See § 4 for a discussion of the best power-law fits and Table 5 for the values.

TABLE 5

BEST-FIT POWER LAW EXPONENT β

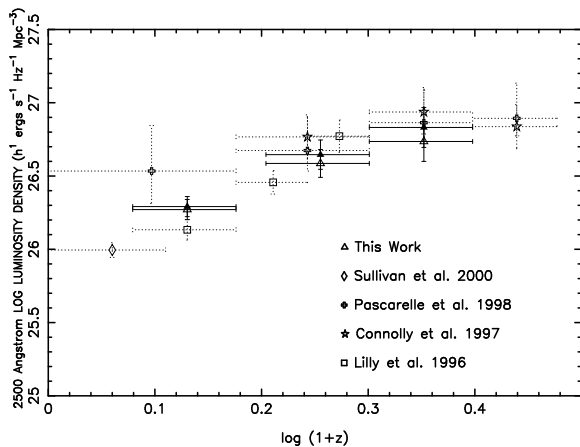| Corrected?	Flat Lambda	Einstein-de Sitter
No	1.44 ± 0.63	2.22 ± 0.62
Yes	1.95 ± 0.65	2.54 ± 0.62

Fig. 7.— $\log_{10}$(Luminosity density) versus $\log_{10}(1 + z)$ for an Einstein de-Sitter cosmology. The triangles are as in Fig. 6 and denote the minimal (open) and incompleteness-corrected (solid) case. The vertical bars show the uncertainties in luminosity density caused by assuming $\alpha = -1.0$ or $\alpha = -1.5$. For comparison we have included data points from Lilly et al. (1996, open squares), Connolly et al. (1997, open star), Pascarelle et al. (1998, open cross) and Sullivan et al. (2000, open diamond).

minosity density to the values obtained by other surveys. Other groups have previously assumed an Einstein-de Sitter cosmology and therefore should be compared to the triangles from Fig. 6. To convert the low-redshift value obtained by Sullivan et al. (2000) (from the FOCA2000 balloon-born survey) we used their best-fit Schechter values (their Table 3) and converted their magnitudes to AB magnitudes using a 2.29 mag offset; we also converted from a rest-frame of 2000 Å to 2500 Å using a $\lambda^{1.1}$ power-law, as suggested by Fig. 4 of CSB. As mentioned in § 1, the Sullivan et al. UV-selected sample results in a higher value of integrated luminosity density for the local universe than previous optically-derived estimates.

In comparing with the surveys of Pascarelle, Lanzetta, & Fernández-Soto (1998), Connolly et al. (1997), and Lilly et al. (1996), we again converted to a rest-frame of 2500 Å using a $\lambda^{1.1}$ power-law. We also converted to $H_0 = 100 \ h \ \mathrm{km \ s^{-1} \ Mpc^{-1}}$, where necessary. Connolly et al. and Pascarelle et al. both calculate their luminosity density from the small Hubble Deep Field North-proper (HDF-N) using photometric redshift estimates. The results of Connolly et al. are more directly comparable to ours since they measure at a rest-frame of 2800 Å whereas Pascarelle et al. measure at a rest-frame of 1500 Å. Connolly et al. assume a faint end slope of $\alpha = -1.3$. Both obtain somewhat higher luminosity densities than do we, although the values are consistent within the uncertainties. As discussed at length in the Appendix to CSB, much of the discrepancy between our results and Connolly et al. and Pascarelle et al. may be attributable to the slightly higher number counts in the HDF-N versus other fields.

Lilly et al. calculated their luminosity density from the Canada-France Redshift Survey, and

found a best-fit exponent of $\beta = 3.9 \pm 0.75$. As discussed in § 1, this is somewhat steeper then the value of $\beta = 2.5 \pm 1.0$ that we obtained. From Fig. 7, we conclude that the steeper value obtained by Lilly et al. is most likely due to a combination of their $z \sim 1$ luminsity density estimate being rather higher than ours, and their use of a low (optically-derived) estimate of the local luminsity density.

In closing, it is important to add one caveat concerning the effect of interstellar dust on our conclusions. In this paper we assumed that any extinction would suppress UV emission uniformly. This corresponds to applying a constant correction factor to the LFs, and does not affect the luminosity density slope inferred from Fig. 7. Some authors have suggested that extinction may be luminosity dependent (Adelberger & Steidel 2000; Sullivan et al. 2000; Hopkins et al. 2001). If this is the case, the higher redshift luminosity functions containing greater contributions from brighter galaxies would see larger extinction corrections, possibly flattening the slope observed in Fig. 7 from a steeper value. The satisfactory resolution of the complex role of dust and the validity of these claims will require further investigation with larger samples.

5. SUMMARY

We investigated the evolution of the universal rest-frame luminosity density from $z = 1.5$ to the present. The availability of both multicolor data and highly complete spectroscopy enabled us to select galaxies based on their rest-frame ultraviolet color, minimizing potential sources of error such as large K-corrections and interstellar dust. Our large, deep sample allowed us to constrain the faint-end of the luminosity function with confidence, even at the highest redshift interval of $z = 1.25 \pm 0.25$. Assuming analytic Schechter forms for our luminosity functions and using likely extremal faint-end slope values of $\alpha = -1.0$ and $\alpha = -1.5$, we constrained the *relative* luminosity density as a function of redshift. We concluded that, in an $\Omega_{m0} = 0.3, \Omega_{\lambda0} = 0.7$ [Einstein-de Sitter] Universe, the evolution in the luminosity density follows a $(1+z)^{1.7\pm1.0}$ $[(1+z)^{2.4\pm1.0}]$ slope from $z = 1.5$ to the present, implying that rather more star formation has occurred in recent times than was previously suggested.

REFERENCES

Adelberger, K. L. & Steidel, C. C. 2000, ApJ, 544, 218

Boyle, B. J., Shanks, T., & Peterson, B. A. 1988, MNRAS, 235, 935

Carlberg, R. G. 1992, ApJ, 399, L31

Connolly, A. J., Szalay, A. S., Dickinson, M., SubbaRao, M. U., & Brunner, R. J. 1997, ApJ, 486, L11

Cowie, L. L., Gardner, J. P., Hu, E. M., Songaila, A., Hodapp, K. W., & Wainscoat, R. J. 1994, ApJ, 434, 114

Cowie, L. L., Songaila, A., & Barger, A. J. 1999, AJ, 118, 603 (CSB)

Efstathiou, G., Ellis, R. S., & Peterson, B. A. 1988, MNRAS, 232, 431

Ellis, R. S., Colless, M. M., Broadhurst, T. J., Heyl, J. S., & Glazebrook, K. 1996, MNRAS, 280, 235

Felten, J. E. 1976, ApJ, 207, 700

Gardner, J. P., Brown, T. M., & Ferguson, H. C. 2000, ApJ, 542, L79

Gehrels, N. 1986, ApJ, 303, 336

Hogg, D. W., Pahre, M. A., McCarthy, J. K., Cohen, J. G., Blandford, R., Smail, I., & Soifer, B. T. 1997, MNRAS, 288, 404

Hopkins, A. M., Connolly, A. J., Haarsma, D. B., & Cram, L. E. 2001, AJ, 122, 288

Lilly, S. J., Cowie, L. L., & Gardner, J. P. 1991, ApJ, 369, 79

Lilly, S. J., LeFèvre, O., Hammer, F., & Crampton, D. 1996, ApJ, 460, L1

Lilly, S. J., Tresse, L., Hammer, F., Crampton, D., & Le Fevre, O. 1995, ApJ, 455, 108

Luppino, G. 1997, in ESO Conference on CCD Detector Technology for Astronomy

Madau, P., Ferguson, H. C., Dickinson, M. E., Giavalisco, M., Steidel, C. C., & Fruchter, A. 1996, MNRAS, 283, 1388

Madau, P., Pozzetti, L., & Dickinson, M. 1998, ApJ, 498, 106

Marshall, H. L. 1985, ApJ, 299, 109

Oke, J. B., Cohen, J. G., Carr, M., Cromer, J., Dingizian, A., Harris, F. H., Labrecque, S., Lucinio, R., et al., 1995, PASP, 107, 375

Page, M. J. & Carrera, F. J. 2000, MNRAS, 311, 433

Pascarelle, S. M., Lanzetta, K. M., & Fernández-Soto, A. 1998, ApJ, 508, L1

Pozzetti, L., Madau, P., Zamorani, G., Ferguson, H. C., & Bruzual, G. 1998, MNRAS, 298, 1133

Sandage, A. J., Tammann, G. A., & Yahil, A. 1979, ApJ, 232, 352

Schechter, P. L. 1976, AJ, 203, 297

Schmidt, M. 1968, ApJ, 151, 393

Sullivan, M., Treyer, M. A., Ellis, R. S., Bridges, T. J., Milliard, B., & Donas, J. 2000, MNRAS, 312, 442

Treyer, M. A., Ellis, R. S., Milliard, B., Donas, J., & Bridges, T. J. 1998, MNRAS, 300, 303

Williams, R. E., Blacker, B., Dickinson, M., Dixon, W. V. D., Ferguson, H. C., Fruchter, A. S., Giavalisco, M., Gilliland, R. L., et al., 1996, AJ, 112, 1335

Wilson, G., Kaiser, N., Luppino, G. A., & Cowie, L. L. 2001, ApJ, 555, 572